NANO LETTERS

Letter

pubs.acs.org/NanoLett

DNA-Assembled Nanoparticle Rings Exhibit Electric and Magnetic Resonances at Visible Frequencies

Eva-Maria Roller,[†] Larousse Khosravi Khorashad,[‡] Michael Fedoruk,[†] Robert Schreiber,[§] Alexander O. Govorov,[‡] and Tim Liedl*[,†]

[†]Fakultät für Physik and Center for Nanoscience, Ludwig-Maximilians-Universität München, Geschwister-Scholl-Platz 1, 80539 Munich, Germany

[‡]Department of Physics and Astronomy, Ohio University, Athens, Ohio 45701, United States

[§]Clarendon Laboratory, Department of Physics, University of Oxford, Parks Road, Oxford OX1 3PU, United Kingdom

Supporting Information

ABSTRACT: Metallic nanostructures can be used to manipulate light on the subwavelength scale to create tailored optical material properties. Next to electric responses, artificial optical magnetism is of particular interest but difficult to achieve at visible wavelengths. DNA-self-assembly has proved to serve as a viable method to template plasmonic materials with nanometer precision and to produce large quantities of metallic objects with high yields. We present here the fabrication of self-assembled ring-shaped plasmonic metamolecules that are composed of four to eight single metal nanoparticles with full stoichiometric and geometric control. Scattering spectra of single rings as well as absorption spectra of solutions containing the metamolecules are used to examine the unique plasmonic features, which are compared to computational simulations. We demonstrate that the electric and magnetic plasmon resonance modes strongly correlate with the exact shape of the structures. In particular, our computations reveal the magnetic plasmons only for particle rings of broken symmetries, which is consistent with our experimental data. We stress the feasibility of DNA self-assembly as a method to create bulk plasmonic materials and metamolecules that may be applied as building blocks in plasmonic devices.

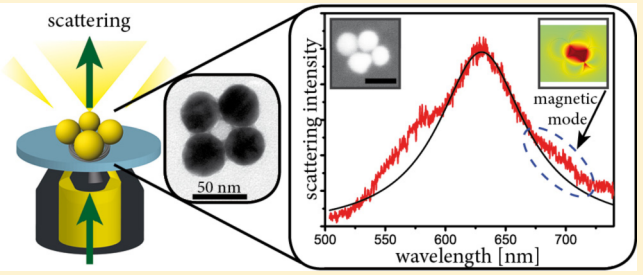

KEYWORDS: *DNA origami, nanoparticles, plasmonic metamaterials, self-assembly*

A negative refractive index metamaterial requires both electric permittivity and magnetic permeability to be negative. While metals naturally exhibit negative real values for their permittivity at visible frequencies, negative permeability has to be created through an "artificial magnetic" response.[1,2] The well-known concept to achieve this goal in the THz domain is to create electric and magnetic resonances in split ring resonators,[3] which has been realized in many examples and led to the development of gradient index lenses[4,5] and switching devices for terahertz radiation.[6] This and similar approaches that are based on electric leads, however, are hard to transfer into the visible frequency domain due to the changing conduction properties of metals at high frequencies and the resulting saturation effect of the magnetic response.[7] As an alternative route to artificial magnetic responses, it has been proposed that metal nanoparticles that are brought together in a ring geometry can support a circulating displacement current induced by plasmonic resonances.[8−10] Similar to the conduction current within split ring resonators the plasmonic interaction can lead to the emergence of magnetic resonances at visible or near-infrared frequencies. Recent implementations of such ring resonators also experimentally demonstrated the appearance of magnetic resonances and even magnetic-based optical Fano resonance.[11] Studies that investigated size- and shape-controlled nanoscale ring arrangements of plasmonic particles used either atomic force microscope nanomanipulation[11] or lithography[12,13] to achieve their goal. Other approaches are based on the use of dielectric spheres as substrates for the random attachment or growth of plasmonic nanoparticles[14−16] or nanoshell clusters.[17,18] To take advantage of the intriguing concept to use plasmonic particle devices as building blocks for large scale metamaterials it is necessary to reach full control over design and manufacturing of subwavelength structures as well as to be able to produce large numbers of plasmonic structures in a parallel manner.

Here we report a strategy to overcome these challenges by using the DNA origami method[19−21] to fabricate versatile templates for metamolecules on a length scale much smaller than the wavelength of visible light. Structural DNA nanotechnology allows the assembly of trillions of identical nanoscale three-dimensional objects at once in a simple, solution-based reaction.[22,23] A DNA origami structure is built

Received: December 3, 2014
Revised: January 16, 2015
Published: January 22, 2015

DOI: 10.1021/nl5046473
Nano Lett. 2015, 15, 1368−1373

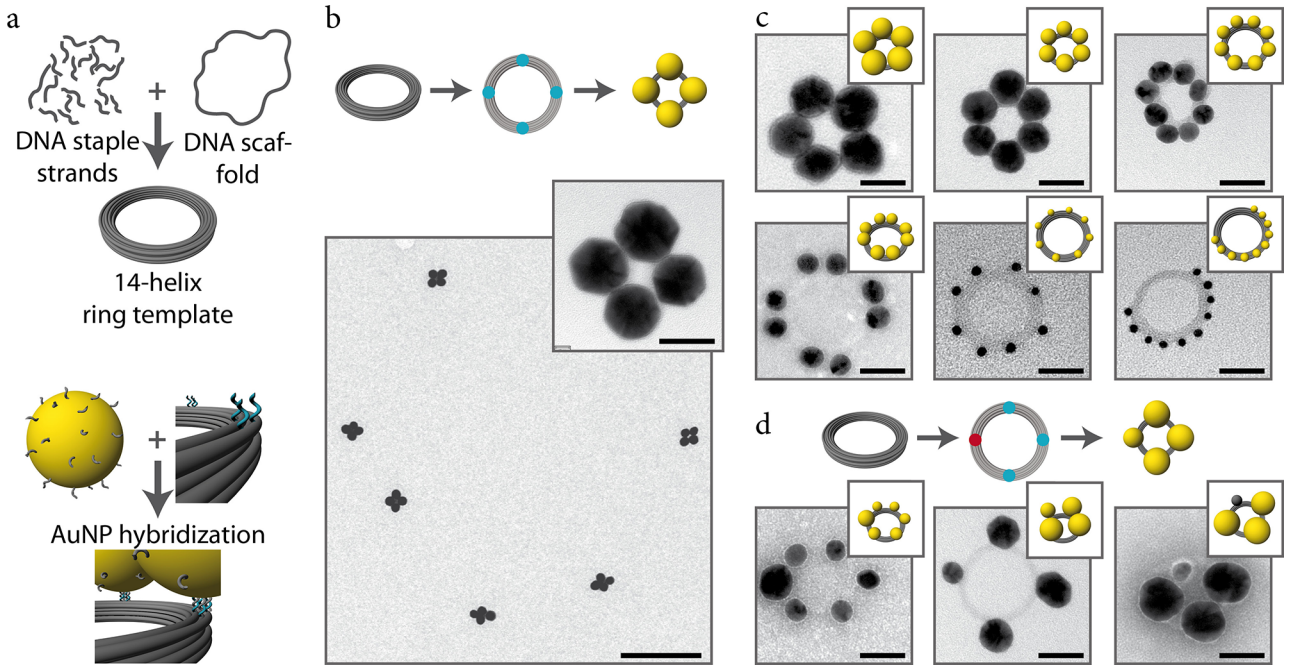

Figure 1. DNA origami–nanoparticle ring structures. Plasmonic rings were built by arranging nanoparticles on ring-shaped DNA origami structures. (a) Self-assembly of DNA origami nanoparticle rings: an 8 kb-long DNA scaffold was annealed with ~250 synthetic staple strands (each ~40 bases long) to create a ring-shaped 14-helix bundle template structure (14HB-template). In the next step, DNA-functionalized AuNPs were attached to defined positions on the 14HB-template via hybridization of the handle sequences protruding from the origami ring and the complementary DNA strands on the AuNPs. (b) Upper panel: schematic illustration of the 14HB-template with four identical attachment sites to create a symmetric four particle ring. Lower panel: Wide-field transmission electron microscopy (TEM) micrograph of plasmonic ring structures consisting of four 40 nm AuNPs. Scale bar: 400 nm. Inset: Zoom-in. Scale bar: 40 nm. (c) Upper panels: Schematic illustration and TEM images of 14HB-templates with five 40 nm AuNPs (left), six 30 nm AuNPs (middle), and eight 20 nm AuNPs (right) attached. Scale bars: 40 nm. Lower panels: Eight 20 nm AuNPs attached in a ring of dimers (left), eight 10 nm AuNPs attached in a ring of equal spacing (middle), and ten 10 nm AuNPs in a C-shaped geometry. Scale bars: 40 nm. (d) Schematic illustration and TEM images of asymmetric ring structure assembly where the attachment sites offer two different sequences (illustrated as red and blue dots). Six (left) and four (middle) AuNPs with two different diameters (30 and 20 nm, and 40 and 20 nm, respectively) are shown, as well as three AuNP and one AgNP (right) with diameters of 40 and 20 nm, respectively.

from one long scaffolding DNA single-strand (here: 8634 nucleotides) that is assembled into the desired two- or three-dimensional shape via the annealing with ~250 short "staple" oligonucleotides. Because of their inherent and defined sequence addressability, DNA structures allow nanometer precise positioning of objects such as metallic nanoparticles through the incorporation of DNA handle sequences at virtually any site on the structures.[24−29]

For our goal to create nanoparticle ring resonators of defined geometries, this bottom-up fabrication method was employed to assemble several nanoring geometries consisting of a defined number of metal nanoparticles that were all equal or of various sizes and materials. Using the software cadnano (cadnano.org)[30] and CanDo[31,32] we designed a ring-shaped DNA-origami structure of 14 parallelly arranged DNA double-helices of 200 nm length that were bent by design[33] into a full circle by insertion and deletion of bases at selected sites (see Supporting Information for design details and experimental protocols S1−S4). The resulting structure has a diameter of 62 nm and a ring cross-section of ~10 nm. To serve as a versatile template for all desirable ring-shaped particle geometries, the DNA origami structure offers repeating units of DNA handles that can act as specific attachment sites for DNA-functionalized nanoparticles, overall 27 evenly spaced sites. It is thus possible to create a large diversity of particle ring geometries. Figure 1 illustrates the self-assembling process and a variety of implemented particle arrangements, including symmetric and asymmetric site-specific organization of particles of different sizes and materials. In the first experimental step, the DNA origami template is annealed by heating up and slowly cooling down a solution containing the scaffold strand and a set of staple oligonucleotides including all sequences that are needed to form the desired attachment sites for particle binding. After purification of the folded DNA origami template via gel electrophoresis, DNA-functionalized gold (AuNP) and silver (AgNP) nanoparticles of the desired size were hybridized to the attachment sites. Here particles of 10−40 nm in diameter were used but in principle also larger and smaller particles could be employed.[26] The AuNPs are covered with 15 nucleotide (nt) long single-stranded DNA (ssDNA) sequences to bind them to the origami template as well as to stabilize them against high salt concentrations that are needed during the annealing process. A second gel electrophoresis step is performed to purify the now assembled metamolecules from the excess of unbound AuNPs and little amounts of aggregated structures (Supporting Information Figure S5). Note that the presence of an excess of nanoparticles during the assembly largely inhibits the aggregation of the metamolecules. We achieved yields of correctly arranged particle rings of up to 73%, (statistics and additional TEM images can be found in the Supporting Information Figures S6−S9). By choosing unique handle sequences at specific attachment sites and by introducing the complementary functionalized particle species, various particle types can be attached at defined positions in one step (Figure 1d) (see Supporting Information for particle functionalization and purification).

DOI: 10.1021/nl5046473
Nano Lett. 2015, 15, 1368−1373

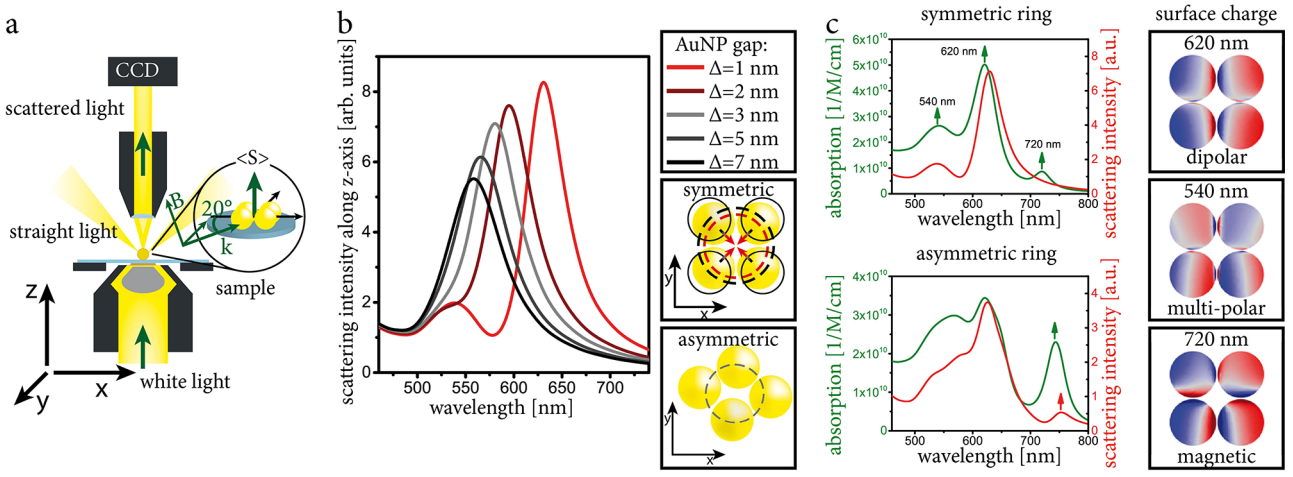

Figure 2. Experimental setup and simulated scattering and absorption spectra of symmetric and asymmetric four-particle ring structures. (a) Experimental dark-field setup and the corresponding model for the numerical simulations (inset). (b) The scattering spectrum of a symmetric ring structure consisting of four 40 nm AuNPs strongly depends on the gap size Δ between the particles. For distances smaller than 4 nm a second resonance peak appears in the scattering spectra. (c) The symmetric ring with a gap size of 1 nm shows two peaks in the scattering simulation but three peaks in the absorption whereas the asymmetric ring shows three peaks both in scattering and absorption. The origins of these peaks are dipolar, multipolar, and magnetic interactions.

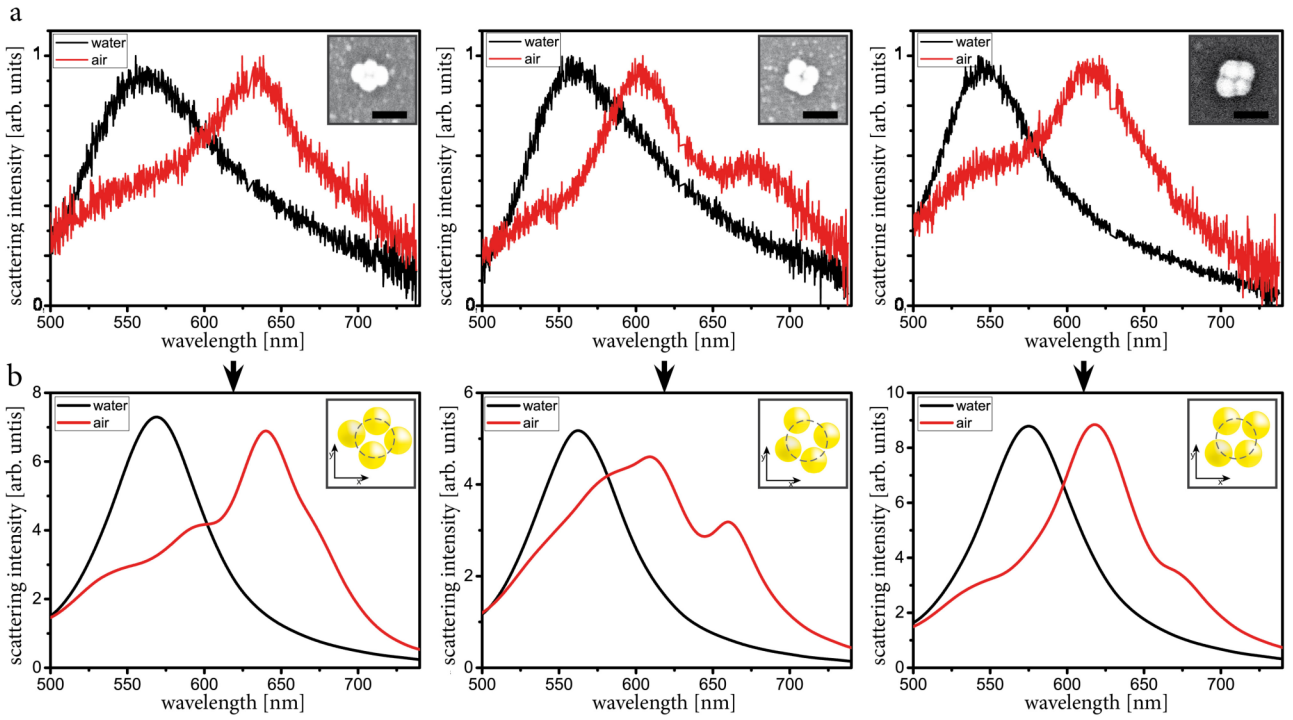

Figure 3. Scattering spectra of individual ring structures immobilized on glass substrates. The spectral shape is strongly dependent on the exact particle ring geometry. (a) Each two scattering spectra were collected from the same structures immersed in buffer (black curves) and after drying in air (red curves). Insets: corresponding SEM images of each ring structure. Scale bar: 100 nm. (b) The spectra in air were simulated with the AuNP positions as determined from SEM data. The spectra in water were then fitted by moving the positions of each AuNP 4 nm radially outward.

Obviously, also smaller and larger ring diameters could be implemented by varying the template DNA structure. The origami template chosen in this study provides a good balance between structural stiffness (cross section) of the ring template and large enough diameter to accommodate the attachment of four or more 30 and 40 nm AuNPs with small gaps between the particles. Importantly, we found in our experiments that small interparticle distances are essential to support circulating current modes along the rings. Because of their comparatively simple spectra, we focus in the following on four-particle metamolecules.

The plasmonic properties of the assembled individual ring structures were characterized by dark-field scattering spectroscopy. In our experimental setup the unpolarized incident light hits the glass substrate at ~23° from all sides and the scattered light is collected above the sample and perpendicular to the glass surface (Figure 2a). First, numerical COMSOL simulations conforming to our experimental geometry were performed to understand the scattering behavior of the particle

DOI: 10.1021/nl5046473
Nano Lett. 2015, 15, 1368–1373

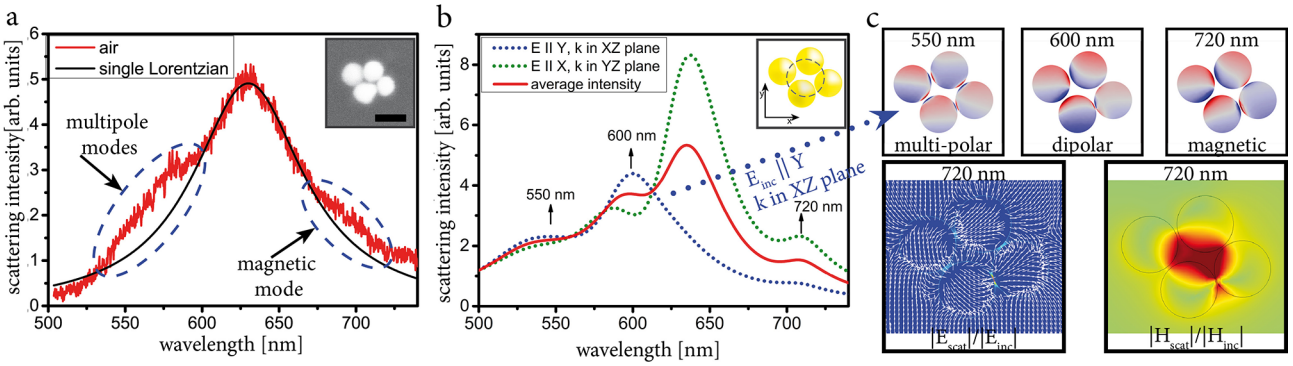

Figure 4. Analysis of single scattering spectrum. (a) Scattering spectra of a structure exhibiting multiple modes. Inset: corresponding SEM image. Scale bar: 50 nm. (b) Simulation of the scattering spectra for different polarizations of the incident light corresponding to the particle ring presented in panel a. Three distinguishable peaks are visible. (c) Simulation of the surface charge distribution for all peaks as well as the electric and magnetic field corresponding to the peak at 720 nm.

rings. In our simulations, we used the empirical dielectric constant of gold taken from Johnson and Christy.[34] Figure 2b shows the simulated scattering spectra for symmetric planar rings consisting of four 40 nm AuNPs. The gap size between the particles was varied between 7 and 1 nm. As observed in previous studies,[35−37] the peak position of the plasmonic resonance shifts to longer wavelengths for smaller gap sizes. Additionally, at gap sizes smaller than 4 nm a second peak becomes distinguishable in the scattering spectra whereas the absorption simulation shows three peaks. We analyzed the three modes in a surface charge intensity plot for the case of 1 nm gaps and found them to originate from dipolar, multipolar, and magnetic interactions (Figure 2c). Interestingly, the rings with perfect symmetry exhibit three modes in the computed absorption spectra, whereas the computed scattering spectra show two modes only and do not show the magnetic mode. However, the simulations executed with slightly asymmetric rings (Figure 2b) do show three distinguishable peaks in both absorption and scattering as here the symmetry breaking induces coupling between the far-field scattered light and the magnetic modes.

To investigate the scattering spectra of the plasmonic ring structures experimentally they were immobilized on a substrate, analyzed with a dark-field spectrometer, and then imaged with scanning electron microscopy (SEM) to determine the exact position of every single AuNP in each ring. For the measurements a droplet of solution containing the ring structures was deposited on a plasma-cleaned quartz glass. After 10 min, the droplet was flushed away by water and the surface was quickly dried with nitrogen. As the particle rings are slightly distorted during the adsorption and the subsequent drying process, small deviations from the designed particle geometries are observed in the SEM images and these spatial variations are in turn reflected in the disparity of the recorded spectra (Figure 3a). To further investigate the influence of the surrounding medium we performed scattering measurements of ring structures in air (red lines in Figure 3a) but also immersed in a buffered solution (1× TBE, 11 mM $MgCl_2$, black lines in Figure 3a).

For structures immersed in solution only one dominant broad resonance at around 560 nm is observed while the spectra taken in air exhibit multiple distinct peaks, as well as a red shift of the dominant resonances. The change of the effective permittivity could explain this red shift[38,39] but not the appearance of the additional resonances. These peaks are a strong indication of a reduction of the interparticle distance,[35,37] which is expected to occur during the drying process, as dehydration will reduce the electrostatic and steric repulsion between the ssDNAs that coat the AuNPs.[38] To study this conformational change of only a few nanometers and to support the experimental observations we performed numerical simulations. The positions of all AuNPs in the dried rings were determined from the SEM images with an accuracy of 1 nm and served as precondition for the simulations. We found an average surface-to-surface distance of 2.4 nm ±1.9 nm (Supporting Information Figure S7) and strikingly, the simulated scattering spectra match the measured spectra of the individual dried structures remarkably well (red lines in Figure 3b). It was also possible to simulate the shape of the experimental spectra collected from the structures immersed in buffer. Therefore, not only the effective permittivity was adapted but also the position of each AuNP had to be moved 4 nm radially outward, which validates the assumption of a shift in the position of the AuNPs during the drying process.

Generally, already small deviations in the positions of the AuNPs compared to a perfect symmetric ring structure cause shifts in the occurring resonant peaks and the emergence of new resonances (cf. simulated spectra in Figure 2b,c and observed and simulated spectra in Figure 3a,b). To analyze the origin of the measured resonances additional numerical simulations were performed for the ring structure shown in Figure 4a. The simulations show three distinguishable peaks in the scattering spectra (Figure 4b). Two peaks (at 550 and 600 nm) were already visible in the symmetric ring case (Figure 2c) and belong to the multipolar and dipolar resonances. The third peak appearing in the computed scattering spectra at 720 nm has its origin in a magnetic plasmon resonance and appears in the scattering configuration only for four-particle rings with broken symmetry. In such asymmetric rings, the magnetic plasmons become active in the scattering because the broken symmetry opens a coupling channel between the magnetic mode and the far-field photons propagating along the *z*-axis. Figure 4c shows the surface charge distributions for all peaks as well as the electric and magnetic field map corresponding to the magnetic resonance at 720 nm. Importantly, the experiments confirm that the response of plasmonic ring structures is very sensitive to their exact geometries and that electric and magnetic resonances can be supported at optical frequencies in our DNA-assembled nanoparticle ring resonators (additional

DOI: 10.1021/nl5046473
Nano Lett. 2015, 15, 1368−1373

spectra can be found in the Supporting Information Figures S10 and S11).

One of the great advantages of DNA-based self-assembly is the possibility to manufacture large numbers of identical objects dispersed in solution, which gives access to the use of the DNA-assembled metamolecules as building blocks in metafluids and to scale up the production.[21,25] To demonstrate that our DNA origami ring structures also perform in liquids, we carried out absorption measurement of bulk solutions containing plasmonic rings with four 40 nm AuNPs. Indeed, the observed spectral peak is shifted from 530 nm for freely dispersed and DNA-coated 40 nm gold nanoparticles to 540 nm for the DNA-assembled particle rings (Figure 5a). The experimental result is in agreement with simulations, which assume an interparticle distance of 10 nm and predict a shift from 530 to 542 nm (Figure 5b).

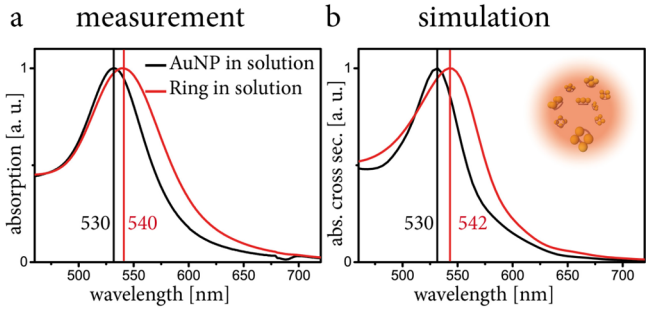

Figure 5. Optical characterization of the bulk plasmonic ring structures in solution. The absorption spectrum of plasmonic ring structures consisting of four 40 nm AuNPs was measured in bulk solution. (a) Measured absorption spectra of 40 nm AuNPs covered with ssDNA (black curve) and the ring structure with four attached 40 nm AuNPs in solution (red curve). (b) Corresponding finite difference time domain (FDTD) simulations of 40 nm AuNP in solution (black curve) and a symmetric ring structure (red curve) with a gap of 10 nm between the AuNP.

Overall, we successfully implemented DNA origami structures as templates for the synthesis of a wide variety of ring geometries containing nanoparticles of selectable size and type. We were able to construct various light-manipulating ring structures with interparticle gaps of only a few nanometers and we demonstrated their ability to support strong plasmonic resonances in the visible frequency domain both attached to a substrate and dispersed in solution. These resonances include dipolar, multipolar, and magnetic modes and are very sensitive to the ring symmetry. Our DNA-based self-assembly approach offers the opportunity to build metamolecules in large numbers with nanometer resolution and dispersed in solutions. This opens the route to a new class of material such as metasprays or metamolecules incorporated in a solid host, which could then be used in nanophotonic and sensing applications.

■ ASSOCIATED CONTENT

Supporting Information

Materials and methods, DNA origami gold nanoparticle attachment, and additional data. This material is available free of charge via the Internet at http://pubs.acs.org.

■ AUTHOR INFORMATION

Corresponding Author

*E-mail: tim.liedl@lmu.de.

Author Contributions

E.M.R., A.O.G., and T.L. designed the research. E.M.R. and R.S. designed the nanostructures. E.M.R. and M.F. performed experiments. E.M.R., L.K., and A.O.G. performed simulations and E.M.R., A.O.G., and T.L. wrote the manuscript.

Notes

The authors declare no competing financial interest.

■ ACKNOWLEDGMENTS

This work was funded by the Volkswagen Foundation, the DFG through the Nanosystems Initiative Munich (NIM), the ERC through the Starting Grant ORCA and the U.S. Army Research Office under Grant W911NF-12-1-0407.

■ REFERENCES

(1) Shalaev, V. M. *Nat. Photonics* **2007**, *1*, 41−48.
(2) Smith, D. R.; Pendry, J. B.; Wiltshire, M. C. K. *Science* **2004**, *305*, 788−792.
(3) Smith, D. R.; Padilla, W. J.; Vier, D. C.; Nemat-Nasser, S. C.; Schultz, S. *Phys. Rev. Lett.* **2000**, *84*, 4184−4187.
(4) Smith, D. R.; Mock, J. J.; Starr, A. F.; Schurig, D. *Phys. Rev. E: Stat., Nonlinear, Soft Matter Phys.* **2005**, *71*, 036609.
(5) Greegor, R. B.; Parazzoli, C. G.; Nielsen, J. A.; Thompson, M. A.; Tanielian, M. H.; Smith, D. R. *Appl. Phys. Lett.* **2005**, *87*, 091114.
(6) Chen, H. T.; Padilla, W. J.; Zide, J. M.; Gossard, A. C.; Taylor, A. J.; Averitt, R. D. *Nature* **2006**, *444*, 597−600.
(7) Zhou, J.; Koschny, T.; Kafesaki, M.; Economou, E. N.; Pendry, J. B.; Soukoulis, C. M. *Phys. Rev. Lett.* **2005**, *95*, 223902.
(8) Alù, A.; Engheta, N. *Phys. Rev. B* **2008**, *78*, 085112.
(9) Alù, A.; Salandrino, A.; Engheta, N. *Opt. Express* **2006**, *14*, 1557−1567.
(10) Campione, S.; Guclu, C.; Ragan, R.; Capolino, F. *ACS Photonics* **2014**, *1*, 254−260.
(11) Shafiei, F.; Monticone, F.; Le, K. Q.; Liu, X.-X.; Hartsfield, T.; Alù, A.; Li, X. *Nat. Nanotechnol.* **2013**, *8*, 95−99.
(12) Nazir, A.; Panaro, S.; Proietti Zaccaria, R.; Liberale, C.; De Angelis, F.; Toma, A. *Nano Lett.* **2014**, *14*, 3166−3171.
(13) Lassiter, J. B.; Sobhani, H.; Fan, J. A.; Kundu, J.; Capasso, F.; Nordlander, P.; Halas, N. J. *Nano Lett.* **2010**, *10*, 3184−3189.
(14) Sheikholeslami, S. N.; Alaeian, H.; Koh, A. L.; Dionne, J. A. *Nano Lett.* **2013**, *13*, 4137−4141.
(15) Sheikholeslami, S. N.; Garcia-Etxarri, A.; Dionne, J. A. *Nano Lett.* **2011**, *11*, 3927−34.
(16) Mühlig, S.; Cunningham, A.; Scheeler, S.; Pacholski, C.; Bürgi, T.; Rockstuhl, C.; Lederer, F. *ACS Nano* **2011**, *5*, 6586−6592.
(17) Fan, J. A.; Bao, K.; Wu, C.; Bao, J.; Bardhan, R.; Halas, N. J.; Manoharan, V. N.; Shvets, G.; Nordlander, P.; Capasso, F. *Nano Lett.* **2010**, *10*, 4680−4685.
(18) Fan, J. A.; Wu, C.; Bao, K.; Bao, J.; Bardhan, R.; Halas, N. J.; Manoharan, V. N.; Nordlander, P.; Shvets, G.; Capasso, F. *Science* **2010**, *328*, 1135−1138.
(19) Rothemund, P. W. K. *Nature* **2006**, *440*, 297−302.
(20) Douglas, S. M.; Dietz, H.; Liedl, T.; Hogberg, B.; Graf, F.; Shih, W. M. *Nature* **2009**, *459*, 414−418.
(21) Kuzyk, A.; Schreiber, R.; Zhang, H.; Govorov, A. O.; Liedl, T.; Liu, N. *Nat. Mater.* **2014**, *13*, 862−866.
(22) Zhang, F.; Nangreave, J.; Liu, Y.; Yan, H. *J. Am. Chem. Soc.* **2014**, *136*, 11198−11211.
(23) Seeman, N. C. *Annu. Rev. Biochem.* **2010**, *79*, 65−87.
(24) Ding, B.; Deng, Z.; Yan, H.; Cabrini, S.; Zuckermann, R. N.; Bokor, J. *J. Am. Chem. Soc.* **2010**, *132*, 3248−3249.
(25) Kuzyk, A.; Schreiber, R.; Fan, Z.; Pardatscher, G.; Roller, E.-M.; Högele, A.; Simmel, F. C.; Govorov, A. O.; Liedl, T. *Nature* **2012**, *483*, 311−314.
(26) Schreiber, R.; Do, J.; Roller, E.-M.; Zhang, T.; Schuller, V. J.; Nickels, P. C.; Feldmann, J.; Liedl, T. *Nat. Nanotechnol.* **2014**, *9*, 74−78.

DOI: 10.1021/nl5046473
Nano Lett. 2015, 15, 1368−1373

(27) Tan, S. J.; Campolongo, M. J.; Luo, D.; Cheng, W. *Nat. Nanotechnol.* **2011**, *6*, 268−276.
(28) Tan, L. H.; Xing, H.; Lu, Y. *Acc. Chem. Res.* **2014**, *47*, 1881−1890.
(29) Zheng, J.; Constantinou, P. E.; Micheel, C.; Alivisatos, A. P.; Kiehl, R. A.; Seeman, N. C. *Nano Lett.* **2006**, *6*, 1502−1504.
(30) Douglas, S. M.; Marblestone, A. H.; Teerapittayanon, S.; Vazquez, A.; Church, G. M.; Shih, W. M. *Nucleic Acids Res.* **2009**, *37*, 5001−5006.
(31) Castro, C. E.; Kilchherr, F.; Kim, D.-N.; Shiao, E. L.; Wauer, T.; Wortmann, P.; Bathe, M.; Dietz, H. *Nat. Methods* **2011**, *8*, 221−229.
(32) Kim, D.-N.; Kilchherr, F.; Dietz, H.; Bathe, M. *Nucleic Acids Res.* **2012**, *40*, 2862−2868.
(33) Dietz, H.; Douglas, S. M.; Shih, W. M. *Science* **2009**, *325*, 725−730.
(34) Johnson, P. B.; Christy, R. W. *Phys. Rev. B* **1972**, *6*, 4370−4379.
(35) Su, K. H.; Wei, Q. H.; Zhang, X.; Mock, J. J.; Smith, D. R.; Schultz, S. *Nano Lett.* **2003**, *3*, 1087−1090.
(36) Jain, P. K.; El-Sayed, M. A. *Chem. Phys. Lett.* **2010**, *487*, 153−164.
(37) Yu, X.; Lei, D. Y.; Amin, F.; Hartmann, R.; Acuna, G. P.; Guerrero-Martínez, A.; Maier, S. A.; Tinnefeld, P.; Carregal-Romero, S.; Parak, W. J. *Nano Today* **2013**, *8*, 480−493.
(38) Thacker, V. V.; Herrmann, L. O.; Sigle, D. O.; Zhang, T.; Liedl, T.; Baumberg, J. J.; Keyser, U. F. *Nat. Commun.* **2014**, *5*, 3448.
(39) Kühler, P.; Roller, E.-M.; Schreiber, R.; Liedl, T.; Lohmüller, T.; Feldmann, J. *Nano Lett.* **2014**, *14*, 2914−2919.

DOI: 10.1021/nl5046473
Nano Lett. 2015, 15, 1368−1373